Journal of Paleontology

www.cambridge.org/jpa

Articles

Cite this article: Cole S.R., Wright D.F., and Hopkins M.J. 2025. Phylogenetic position and stratigraphic uncertainty of a new flexible crinoid from the Ordovician–Silurian boundary of Anticosti Island (Québec, Canada). *Journal of Paleontology*, 1–11
https://doi.org/10.1017/jpa.2025.10110

Received: 03 December 2024
Revised: 21 April 2025
Accepted: 25 April 2025

Corresponding author:
Selina R. Cole;
Email: colesr@ou.edu

Handling Editor:
Przemyslaw Gorzelak

JOURNAL OF PALEONTOLOGY
A PUBLICATION OF THE Paleontological SOCIETY

CAMBRIDGE UNIVERSITY PRESS

Phylogenetic position and stratigraphic uncertainty of a new flexible crinoid from the Ordovician–Silurian boundary of Anticosti Island (Québec, Canada)

Selina R. Cole[1,2,3], David F. Wright[1,2,3] and Melanie J. Hopkins[3]

[1]Sam Noble Oklahoma Museum of Natural History, University of Oklahoma, 2401 Chautauqua Avenue, Norman, OK, 73072, USA
[2]School of Geosciences, University of Oklahoma, 100 E Boyd Street, Norman, OK, 73019, USA
[3]Division of Paleontology (Invertebrates), American Museum of Natural History, New York, NY 10024, USA

Abstract

Fossil crinoids from the Ordovician–Silurian boundary interval (~ 443.8 million years) are known from relatively few locations worldwide due to a near-global unconformity that formed from eustatic sea-level fall. This rock record bias has severely hindered study of the timing, magnitude, biogeographic signature, and extinction mechanisms of the Late Ordovician mass extinction (LOME). Crinoids underwent a significant faunal transition between the Late Ordovician and early Silurian that resulted in major shifts between dominant clades, but the driving mechanisms and precise timing of this transition remain unclear. Anticosti Island (Québec, Canada) preserves one of the few Late Ordovician–early Silurian successions of highly fossiliferous, shallow-water rocks that includes the Ordovician–Silurian boundary, making fossils from this region instrumental for better understanding the LOME and Ordovician–Silurian crinoid faunal turnover.

Here we report on a new flexible crinoid, *Anticosticrinus natiscotecensis* n. gen. n. sp., from the Ordovician–Silurian boundary of Anticosti Island. Phylogenetic analysis of Middle Ordovician–early Silurian flexibles recovers *Anticosticrinus natiscotecensis* n. gen. n. sp. as a member of family Anisocrinidae. We quantified stratigraphic age uncertainty of *A. natiscotecensis* using a Bayesian approach for estimating tip-occurrence times in a phylogenetic context. Although results do not provide unequivocal support for the specimen's precise stratigraphic age, the maximum a posteriori estimate indicates a late Hirnantian age. Regardless of its true age, recognition of *Anticosticrinus natiscotecensis* provides additional data for evaluating the timing of extinction in flexible crinoids, their diversification and increasing dominance during the Silurian, and crinoid faunal turnover between the Ordovician and Silurian.

UUID: http://zoobank.org/864738dd-3fc9-435b-a83c-e19fd4f6Ad9d

Non-technical Summary

The Late Ordovician mass extinction (LOME) was the first of the "Big Five" extinction events in the history of life. Crinoids, a major group of marine animals related to starfish and sea urchins, were significantly affected by this extinction event, and the species composition of crinoid communities exhibits dramatic differences before and after the extinction. However, the precise timing and severity of crinoid extinction and the nature of community change have remained unclear because there are few outcrops worldwide preserving fossils from the extinction interval. As a result, the discovery of new fossils from the time when the LOME occurred can provide crucial insight into this extinction event. Here we describe a new genus and species of fossil crinoid, *Anticosticrinus natiscotecensis*, that is from the time interval of the LOME on Anticosti Island, Québec (Canada). We conduct a series of analyses to identify the evolutionary relationships between *Anticosticrinus* and other closely related crinoids in the lineage known as the Flexibilia and constrain the likely age of the fossil to the latest part of the extinction event. The discovery of *Anticosticrinus natiscotecensis* and results of our analyses provide new information on how crinoids were impacted by LOME and recovered in its aftermath.

Introduction

The Ordovician–Silurian transition was a key interval in the evolutionary history of crinoids. During the Middle to Late Ordovician, crinoids underwent substantial taxonomic, morphological, and ecological diversification as part of the Great Ordovician Biodiversification Event (Foote 1995, 1999; Deline and Ausich, 2011; Wright and Toom, 2017; Cole, 2019; Cole et al., 2019, 2020; Cole and Wright, 2022; Novack-Gottshall et al., 2022, 2024). Crinoids subsequently suffered heavy losses during the Late Ordovician mass extinction (LOME), which was the second-most

severe mass extinction event in Earth's history (Sepkoski, 1996; Alroy et al., 2008; Peters and Ausich, 2008; Harper et al., 2014), and experienced a significant decrease in body size, referred to as the "Lilliput Effect" (Harries and Knorr, 2009; Borths and Ausich, 2011; Salamon et al., 2023). In the aftermath of the LOME, crinoids underwent a major radiation during the early–middle Silurian (Peters and Ausich, 2008; Wright and Toom, 2017; Cole, 2019). In response to these events, crinoid faunas experienced a major macroevolutionary turnover from the early Paleozoic Crinoid Evolutionary Fauna (CEF) to the middle Paleozoic CEF around the Ordovician–Silurian transition (Baumiller, 1992; Ausich et al., 1994), with differential extinction combined with long-term ecological pressures implicated as major drivers (Ausich and Deline, 2012; Cole and Wright, 2022). This discontinuity in crinoid evolutionary history resulted in substantial shifts in community composition and clade dominance from diplobathrids, disparids, and hybocrinids during the early Paleozoic CEF to monobathrids, cladids, and flexibles during the middle Paleozoic CEF (Ausich et al., 1994; Ausich and Deline, 2012), in addition to changes in diversity, morphology, and local abundance of crinoid clades.

Despite the importance of the Ordovician–Silurian transition in understanding crinoid evolutionary history, diversification dynamics, and patterns of morphological evolution, these efforts have been hindered by a lack of data from the Hirnantian (latest Ordovician) and Llandovery (earliest Silurian). In part, this paucity of data is due to the nature of the LOME, which was partially driven by a massive, eustatic fall in sea level that resulted in a major unconformity that spans the Ordovician–Silurian boundary in much of the global rock record (Harper et al., 2014). Anticosti Island (Québec, Canada) is one of only a few locations globally that preserves near-continuous deposition from the Late Ordovician through the early Silurian, making it an important region for documenting biodiversity patterns across the LOME and during the subsequent post-extinction recovery (Chatterton and Ludvigsen, 2004; Jin and Zhan, 2008; Ausich and Copper, 2010).

Here we describe *Anticosticrinus natiscotecensis* n. gen. n. sp., a new flexible crinoid from Anticosti Island. Phylogenetic analyses are conducted to identify the taxonomic affinities of this new crinoid, and a fossilized birth–death (FBD) divergence dating analysis is used to constrain the probable age of the specimen on the basis of its phylogenetic position and stratigraphic occurrences of sister taxa. Results shed light on patterns of crinoid extinction and diversification surrounding the LOME and Silurian radiation and contribute to a deeper understanding of clade dynamics and faunal turnover during this critical interval.

Stratigraphy and geologic setting

Anticosti Island (Québec, Canada) is one of only a few locations globally that preserves a largely complete sequence of fossiliferous strata spanning the Ordovician–Silurian boundary. The oldest rocks preserved on Anticosti Island belong to the Katian-aged Vaureal Formation, which is overlain by the Ellis Bay Formation (Hirnantian, latest Ordovician) and Becscie Formation (Rhuddanian, earliest Silurian) (Fig. 1). This succession is dominated by storm-influenced carbonate sediments with increasing siliciclastic content to the east, which were deposited in a foreland basin on the eastern margin of Laurentia around a paleolatitude of 15–20°S (Long, 2007; Mauviel et al., 2020). Despite eustatic sea-level fall during the Late Ordovician, continued subsidence of the basin and consistent sediment supply resulted in the expanded Ordovician–Silurian boundary section that is now exposed on Anticosti Island (Long, 2007; Mauviel et al., 2020). The rocks of Anticosti Island have essentially no structural overprinting but dip gently to the southwest due to the original angle of deposition (Desrochers et al., 2010). As a result, the western and central portions of the island preserve storm-dominated siliciclastic–carbonate facies that represent offshore environments, whereas the

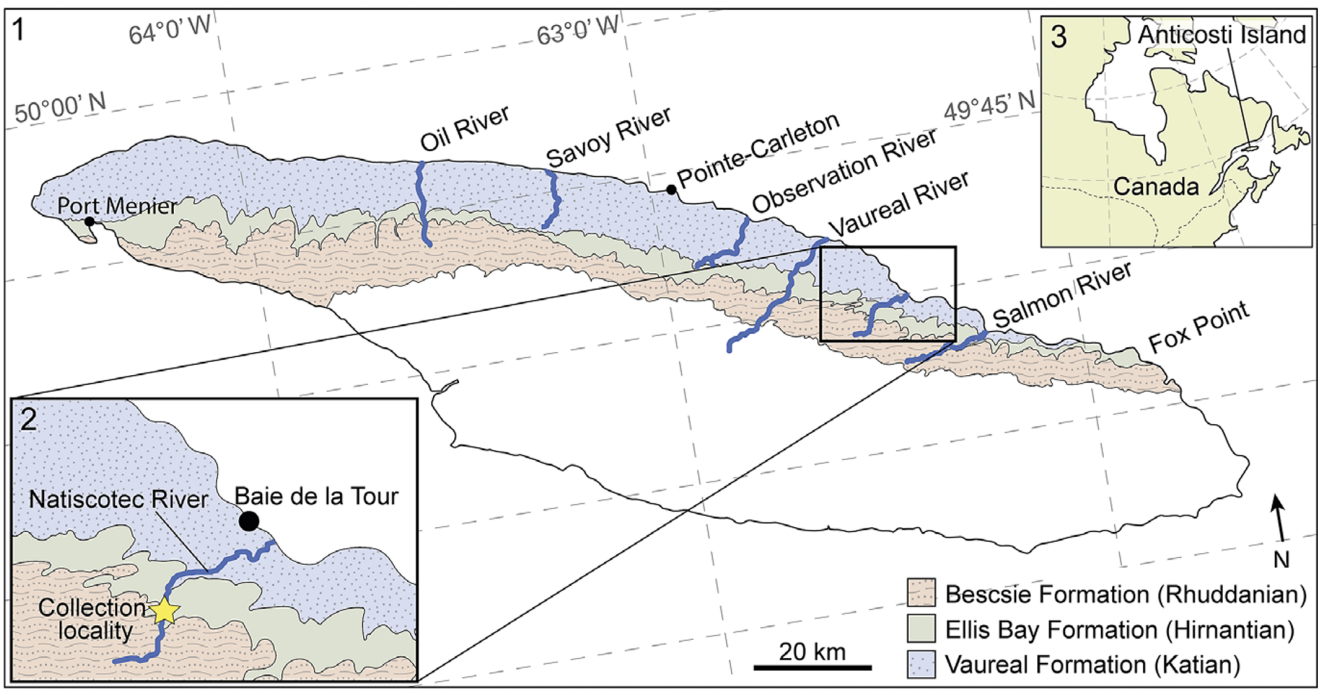

Figure 1. Locality map. (**1**) Major landmarks and bedrock geology of Anticosti Island showing the distribution of Katian to Rhuddanian strata. (**2**) Collection location of *Anticosticrinus natiscotecensis* n. gen. n. sp. (indicated by star) along the Natiscotec River. (**3**) Regional map showing the location of Anticosti Island.

https://doi.org/10.1017/jpa.2025.10110 Published online by Cambridge University Press

eastern end of the island preserves mixed storm-dominated siliciclastic–carbonate facies that represent shallower, proximal shore environments.

Locality and age information. The new crinoid described here was collected from the Natiscotec River (49°28'47"N, 62°30'46"W) during fieldwork by the authors in 2019 (Fig. 1). The mouth of the Natiscotec River opens on the northern coast of Anticosti Island, approximately 1.5 km southeast of Baie de la Tour and 70 km from the eastern end of the island, and it extends about 10 km inland to the southwest. Stratigraphically, the lowest unit exposed along the Natiscotec River is the Vaureal Formation near the coast, while upstream the Ellis Bay and Becscie formations are exposed. The crinoid described here was collected as float in the Natiscotec River, adjacent to Hirnantian-aged rocks of the Ellis Bay Formation. As a result, the stratigraphic position of the specimen is constrained to the Ellis Bay or Becscie formations, but the exact age is unknown because the specimen may have been transported from younger, Rhuddanian-aged strata upstream. To further constrain its possible age, we applied methods commonly used in phylogenetic divergence dating analyses to probabilistically estimate the age of *Anticosticrinus natiscotecensis*.

Materials and methods

Specimen preservation and preparation. The single crinoid specimen examined in this study is preserved as a three-dimensional specimen, with small amounts of matrix preserved between rays of the crinoid. The matrix associated with the specimen is a mica-rich carbonate siltstone. The specimen was prepared using air abrasion with iron powder.

Phylogenetic analyses. Phylogenetic analyses using both maximum parsimony and Bayesian methods were conducted to inform the higher taxonomic assignment of *Anticosticrinus natiscotecensis* n. gen. n. sp. and to clarify its phylogenetic position among Ordovician–Silurian flexible crinoids. The most recent phylogenetic analysis of flexible crinoids was a genus-level analysis conducted by Wright and Toom (2017) using a morphological character matrix that included 25 characters and nine taxa sampled from the Ordovician to middle Silurian. We re-evaluated all coded characters and expanded the matrix of Wright and Toom (2017) to sample *Anticosticrinus* as well as two additional flexible crinoids from the time interval of our primary focus: *Anisocrinus prinstaensis* Ausich and Copper, 2010 from the Hirnantian of Anticosti Island and *Kyphosocrinus tetraulti* Eckert and Brett, 2001 from the Llandovery of New York. The resulting morphological character matrix consisted of 12 taxa and 25 characters, with *Cupulocrinus* designated as the outgroup to the Flexibilia (Springer, 1920; Wright, 2017).

A maximum-parsimony analysis was conducted in PAUP* v4.0a149 (Swofford, 2003) using a branch-and-bound maximum-parsimony analysis that comprehensively searches treespace for the most parsimonious tree topologies, which was possible due to the relatively small size of the matrix. To evaluate support for recovered topologies, jackknife values (using a branch-and-bound search with 100 replicates and 20% deletion) and bootstrap values (using a branch-and-bound search with 100 replicates and all characters resampled) were also calculated in PAUP*.

We also inferred evolutionary relationships using Bayesian methods. Likelihoods for character evolution were calculated according to the Mk model of Lewis (2001), and a compound Gamma Dirichlet prior distribution was placed on the tree length and branch lengths (Rannala et al., 2012; Zhang et al., 2012). The posterior distribution was estimated using Markov chain Monte Carlo (MCMC) simulation in MrBayes 3.2.6 (Ronquist et al., 2012). Two MCMC runs with two chains were run for 1 million generations. Chains were sampled every 100 generations, and the first 25% of samples were discarded as burn-in. Chains reached an average deviation of split frequencies < 0.01. Convergence diagnostics were visually inspected in Tracer 1.7.1 (Rambaut et al., 2018) and by examining the effective sample sizes and potential scale reduction factor values of parameters (Ronquist et al., 2012). Node support was evaluated by examining their posterior probability (PP), which is calculated as the frequency of clades recovered across the posterior distribution.

Age analyses. Because *Anticosticrinus natiscotecensis* n. gen. n. sp. was collected from float and a precise age assignment could not be determined on the basis of stratigraphic context alone, a phylogenetic divergence dating analysis was conducted to better constrain its stratigraphic position and estimate a probability distribution of its age. On the basis of the regional context where *Anticosticrinus* was found, minimum and maximum possible ages were identified and used to calibrate priors on the stratigraphic range of the specimen's occurrence. The specimen was recovered from gravel in the Natiscotec River adjacent to in situ rocks from the Ellis Bay Formation, which constrains the maximum age to be Hirnantian. The specimen was likely transported from strata exposed farther upstream, which would be stratigraphically upsection from where it was discovered. Upstream, the youngest rocks through which the Natiscotec River passes belong to the Becscie Formation, which is lower Silurian (Rhuddanian) in age. As a result, we placed a broad, uniform prior distribution on the tip age interval of *Anticosticrinus natiscotecensis*, reflecting the wide range of potential taxon sampling intervals from strata ranging in age from the base of the Hirnantian (445.2 Ma) to the top of the Rhuddanian (440.8 Ma), with numerical ages based on those assigned for geologic stages in the 2023 International Chronostratigraphic Chart (Cohen et al., 2023).

To generate an evolutionary timescale for flexible evolution and quantify the uncertain stratigraphic age of our *A. natiscotecensis* specimen, we conducted a Bayesian phylogenetic divergence dating analysis incorporating the FBD process (Stadler, 2010; Heath et al., 2014; Wright, 2017; Wright et al., 2021). Bayesian phylogenetic methods using FBD models leverage both morphological and stratigraphic age information from the fossil record (Barido-Sottani et al., 2020; Wright et al., 2021) and can be used to infer evolutionary relationships, estimate divergence times and tip ages for fossil taxa, or both simultaneously. We applied the sampled-ancestor implementation of the FBD model (Gavryushkina et al., 2014) and placed broad priors on FBD parameters for diversification, extinction, and fossil sampling. Species ages were assigned uniform distributions on the basis of their first-appearance occurrence intervals in geologic stages. To assist the analysis and improve FBD parameter estimation (Wright et al., 2021; Barido-Sottani et al., 2023), we applied a topological constraint to reflect the consensus topology resulting from the parsimony and undated Bayesian phylogenetic analyses, and subsequently added an additional 17 species of early Paleozoic flexibles using taxonomic structure to inform clade constraints following the procedure in Wright and Toom (2017). As in the undated Bayesian analysis, morphological character evolution was modelled using a simple Markov model (Lewis, 2001). However, we also accounted for rate variation among lineages throughout the tree by applying an uncorrelated

https://doi.org/10.1017/jpa.2025.10110 Published online by Cambridge University Press

morphological clock where branch rates vary according to an independent gamma rates model (Lepage et al., 2007).

Bayesian estimation of divergence times and tip ages was performed using MCMC simulation in MrBayes 3.2.6 (Ronquist et al., 2012). Two MCMC runs with four chains were run for 10 million generations. Chains were sampled every 5,000 generations, and the first 25% sampled were discarded as burn-in. As for the undated analysis, MCMC convergence was assessed by inspecting trace plots in Tracer 1.7.1 (Rambaut et al., 2018) and by checking the effective sample sizes and potential scale reduction factors of parameters.

Repositories and institutional abbreviations. The specimen described in this study is reposited in the Fossil Invertebrates collections at the American Museum of Natural History (AMNH), New York, USA, under catalog number AMNH-FI-139850.

Additional referenced specimens are from the University of Michigan Museum of Paleontology (UMMP); the Department of Geology at Tallinn University of Technology, Estonia (GIT); the Geological Survey of Canada (GSC); the Buffalo Museum of Science (BMS); and the Field Museum of Natural History (UC).

Systematic paleontology

Classification and terminology. The higher classification of crinoids used here follows Ausich et al. (2015) and Wright et al. (2017). Morphologic terminology follows Ubaghs (1978), Wright (2015), and Ausich et al. (2020).

Class **Crinoidea** Miller, 1821
Subclass **Pentacrinoidea** Jaekel, 1918
Infraclass **Inadunata** Wachsmuth and Springer, 1885
Parvclass **Cladida** Moore and Laudon, 1943
Superorder **Flexibilia** von Zittel, 1895
Order **Sagenocrinida** Springer, 1913
Superfamily **Sagenocrinitacea** Roemer, 1854
Family **Anisocrinidae** Eckert and Brett, 2001

Included genera. Five genera have been assigned to Anisocrinidae, and as currently known, the family persisted from the Katian to Ludlow on the paleocontinents of Laurentia and Baltica. *Anisocrinus* Angelin, 1878 is known from the Hirnantian of Québec (Canada), Wenlock of Sweden and Indiana (USA), and Wenlock–Ludlow of Tennessee and Kentucky (USA); *Cryptanisocrinus* Donovan et al., 1992 is known from the Telychian (upper Llandovery) of Ireland; *Kyphosocrinus* Eckert and Brett, 2001 is known from the Telychian (upper Llandovery) of New York (USA); *Paranisocrinus* Frest and Strimple, 1978 is known from the Ludlow of Sweden; and *Proanisocrinus* Frest and Strimple, 1978 is known from the Katian of Illinois (USA). *Anticosticrinus natiscotecensis* n. gen. n. sp. is the second anisocrinid recognized from Québec, Canada. Given the uncertainty in the specimen's exact age around the Ordovician–Silurian boundary, it is either the second anisocrinid known from the Hirnantian or the first known from the Rhuddanian.

Emended diagnosis. Sagenocrinitaceans with short ovoid crown; infrabasals visible in lateral view; radianal typically present, pentagonal, situated directly below C ray radial; anal X succeeded by additional plates in some instances; distal arms isotomous to slightly heterotomous in some instances; interbrachials absent or consisting of one to several plates in each interray; fixed intrasecundibrachials and intratertibrachials may be present (diagnosis emended from Eckert and Brett, 2001).

Remarks. Anisocrinidae was established by Eckert and Brett (2001) to replace the subfamily Anisocrininae that was defined by Frest and Strimple (1978). The phylogenetic analysis presented here provides further support for the validity of this family (see Phylogenetic results). The new addition of *Anticosticrinus* to Anisocrinidae requires only a minor emendment to include the presence of fixed intrasecundibrachials and intratertibrachials in the original family diagnosis of Eckert and Brett (2001).

Genus ***Anticosticrinus*** new genus

Type species. Anticosticrinus natiscotecensis new species, by monotypy.

Diagnosis. As for species, by monotypy.

Occurrence. As for species.

Etymology. The genus *Anticosticrinus* is named for Anticosti Island, Québec, where the only known specimen has been found.

Remarks. The firmly interlocking interray and proximal fixed brachial plates of *Anticosticrinus* n. gen. along with the presence of a radianal directly below the C radial and large anal X in the posterior interray identify it as a member of Order Sagenocrinida. *Anticosticrinus* is assigned to family Anioscrinidae on the basis of the visibility of infrabasals in lateral view, the presence of a pentagonal radianal directly below the C radial, the anal X followed by additional posterior plates, interrays primarily reduced to a single large plate, and isotomous arm branching (Eckert and Brett, 2001). In addition to these skeletal morphological features, phylogenetic analyses consistently recover *Anticosticrinus* as being sister to *Anisocrinus* and closely related to other anisocrinids (see Results), which further supports its assignment to Anisocrinidae.

Morphologically, *Anticosticrinus* is most similar to *Anisocrinus*, which includes the Hirnantian-aged species *A. prinstaensis*, which also occurs on Anticosti Island (Ausich and Copper, 2010). Both taxa possess a similar posterior interray configuration with a pentagonal radianal positioned directly below the C radial, the anal X in contact with the upper left side of the radianal, and two or more additional posterior plates directly above the anal X. Both taxa also have regular interrays that are primarily made up of single large plates that rest on the shoulders of the underlying radials. However, *Anticosticrinus* differs in that the brachials are fixed through the proximal tertibrachials; fixed intrabrachials are present between half and quarter rays at the height of the secundibrachials and tertibrachials; and rounded to triangular projections extend laterally from the brachials. By contrast, *Anisocrinus* has brachials that are fixed only through the secundibrachials; fixed intrabrachials are absent; and brachials lack lateral projections.

Anticosticrinus is also similar to the monospecific genus *Kyphosocrinus* Eckert and Brett, 2001 known from the middle Llandovery (Telychian) of New York. Both genera have a pentagonal radianal positioned directly below the C radial, anal X in contact with the radianal and positioned to the upper left, and a single plate comprising the majority of the interrays. *Anticosticrinus* differs from *Kyphosocrinus* in that it has a straight-sided conical calyx; infrabasals circlet that is flat in lateral profile; at least two large posterior plates above the anal X; a single very large plate that dominates each interray, with or without the addition of small accessory plates; fixed intrabrachials between half rays and quarter rays; and poorly isotomous branching throughout the arms. By contrast, *Kyphosocrinus* has a calyx that is obconical, infrabasals circlet that bulges in

https://doi.org/10.1017/jpa.2025.10110 Published online by Cambridge University Press

lateral profile, lack of additional posterior plates or with a variable number of small accessory plates above the anal X, interrays typically composed of a single very small interray plate that may include additional accessory plates above, no fixed intrabrachials, and isotomous branching proximally transitioning to endotomous branching in higher arms.

Anticosticrinus natiscotecensis new species
Figures 2, 3

Type material. AMNH-FI-139850, the holotype and only known specimen.

Diagnosis. Anisocrinid with elongate ellipsoidal crown; regular interrays consisting of a single, large plate; radianal pentagonal, positioned directly below the C radial; anal X in contact with the upper left side of the radianal; at least two additional plates positioned directly above the anal X; firmly interlocking proximal brachials and interray plates; brachials fixed through the proximal tertibrachials; fixed intrabrachial plates between half rays and quarter rays; brachial plates with laterally extending rounded to triangular projections.

Occurrence. The holotype and only known specimen of *A. natiscotecensis* is from the Natiscotec River, Anticosti Island, Québec.

Description. Crown large (maximum width 40 mm; maximum height 65 mm), elongate ellipsoidal. Aboral cup medium cone shape, straight-sided, distal width-to-height ratio approximately 1:1; calyx base upright. Plate sutures flush with plate surfaces; fine, rugose ridges ornamenting interray plates, intrabrachials, fixed brachials, and at least proximal free brachials (Fig. 2.10). Fixed brachials raised and broadly convex; E radial with inverted V-shaped ridge extending onto adjacent DE and EA basals (Fig. 2.3), presumably present on all rays but lost due to weathering.

Infrabasal circlet slightly visible in side view, comprising approximately 5% of total aboral cup height. Infrabasals three, all wider than high; azygous infrabasal roughly quadrangular, diamond-shaped, in C ray position; zygous infrabasals pentagonal (Fig. 2.11). Basal circlet approximately 20% of aboral cup height. Basal plates five, slightly wider than high, irregular in shape but roughly pentagonal to heptagonal; CD basal largest, similar in size to radials, truncated distally; other basals smaller than radials by approximately 25–50%, tapering distally to a point (Fig. 3.1). CD basal in sutural contact with infrabasals proximally, C radial and radianal laterally, and anal X distally; all other basals in sutural contact with infrabasals proximally, other basals laterally, and radials distally (Fig. 2.9).

Radial circlet entirely visible in side view, approximately 22% of aboral cup height; radials in sutural contact with each other laterally, circlet interrupted in CD interray only. Radial plates five, wider than high, largest plates in calyx, somewhat unequal in size, with E radial being the largest; A, B, and E radials heptagonal, C and D radials hexagonal (Fig. 3.1). C radial plate truncated proximally by contact with underlying radianal plate.

Regular interrays depressed between fixed brachials, resting on upper shoulders of radial plates, not in contact with tegmen or infrabasals. Interrays composed of a single, large interray plate, similar in size to basals, distally in contact with first secundibrachials; interray plates elongated ellipsoids, much higher than wide, irregularly shaped but roughly heptagonal or octagonal; AE interray includes a very small additional plate on the upper left side (Figs. 2.3, 3.1).

Posterior interray with three anal plates at least partially in aboral cup. Radianal pentagonal, wider than high, similar in shape to but smaller than radial plates, positioned immediately below C radial. Anal X heptagonal, slightly wider than high, positioned directly above CD basal and in sutural contact with upper left shoulder of radianal (Fig. 3.1). Radianal followed by one anal plate in aboral cup; at least two, but likely three or more, additional fixed posterior plates one above the other (Fig. 2.5, 2.9).

Brachials fixed through the proximal tertibrachials (Fig. 3.2). Primibrachials fixed, second primibrachial axillary; first primibrachials quadrangular or hexagonal, approximately 1.5 times wider than high; primaxil approximately 1.75 times wider than high. Secundibrachials fixed, third secundibrachial axillary, secundaxil approximately 1.8 times wider than high, nonaxillary secundibrachials approximately 1.6 times wider than high. Proximal tertibrachials approximately 1.8 times wider than high, fixed through about the third tertibrachial. Fixed secundibrachials with distinctive rounded to triangular projections extending abmedially from each half ray; projections continuing onto fixed tertibrachials and quartibrachials both abmedially and admedially from quarter rays, becoming increasingly indistinct distally (Fig. 2.4, 2.6).

Fixed intrabrachials present between secundibrachials of half rays, consisting of a single plate that may be followed by one or two additional smaller plates (Fig. 2.1, 2.3), and between tertibrachials of quarter rays, consisting of one or two small plates stacked in a vertical column (Figs. 2.6, 3.1).

Free arm openings 20, four per ray, distributed evenly around the margin of the calyx. Free brachials rectilinear uniserial, wider than high proximally, more equant distally; brachials with distinctive rounded to triangular projections extending from the margins, creating a serrated appearance. Projections become less pronounced distally within the free quartibrachials and above and disappear entirely in the distalmost arms. All free arms branching poorly isotomously once, with extensive variability in the height of the branching point (Fig. 3.2); branching points roughly symmetric on either side of each ray axis; all bifurcations give rise to arms of equal size.

Lumen appears to be weakly trilobate (Fig. 2.11). Details of tegmen, column, and holdfast unknown.

Etymology. The species name is given in reference to the Natiscotec River on Anticosti Island, where the only known specimen has been found.

Remarks. Both the position of the radianal directly beneath the C radial and an anal X that is smaller than the radial plates are considered primitive conditions in anisocrinids (Frest and Strimple, 1978; Ausich and Copper, 2010). The presence of both of these conditions in *Anticosticrinus*, which is one of the oldest known anisocrinids, is consistent with the interpretation that this is the ancestral condition of the family. These features are also shared by the oldest known species of *Anisocrinus*, *A. prinstaensis*, which further supports the hypothesis that these conditions are typical of early anisocrinid morphology.

The only known specimen of *A. natiscotecensis* n. gen. n. sp. has two dark markings on the calyx that are both approximately 2.5 mm in diameter. The first of these markings is positioned on the left side of the B radial plate (Fig. 2.7) and appears to be a bore hole of the

https://doi.org/10.1017/jpa.2025.10110 Published online by Cambridge University Press

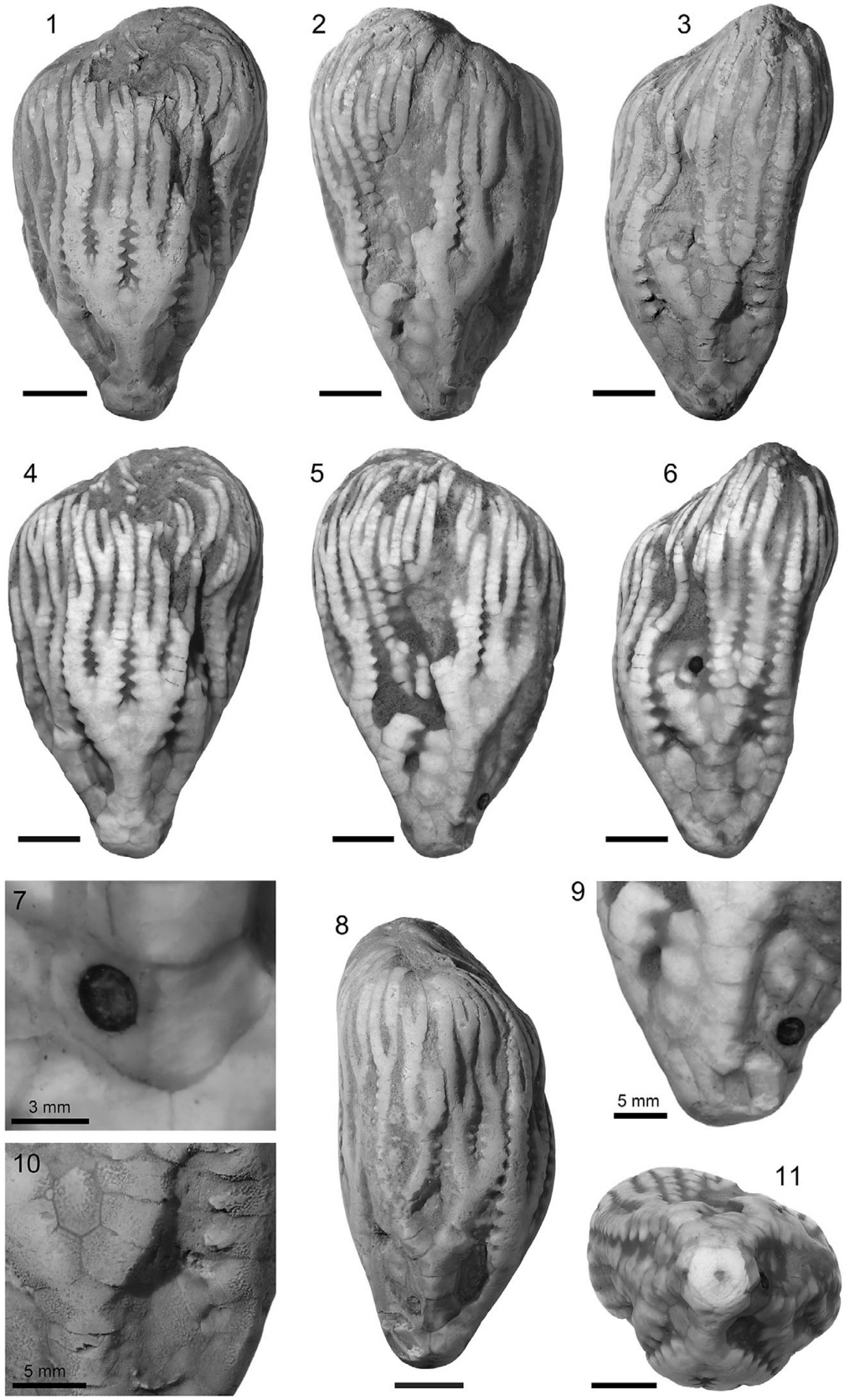

Figure 2. *Anticosticrinus natiscotecensis* n. gen. n. sp., AMNH-FI-139850, from Anticosti Island, Québec. (**1**) Lateral view of A ray whitened with ammonium chloride. (**2**) Lateral view of CD interray whitened with ammonium chloride. (**3**) Lateral view of E ray whitened with ammonium chloride. (**4**) Lateral view of A ray photographed under alcohol. (**5**) Lateral view of CD interray photographed under alcohol. (**6**) Lateral view of E ray photographed under alcohol; note dark, circular structure on tertibrachials. (**7**) Closeup of B-ray radial showing a second dark, indented circle that may represent a drill hole or parasitic interaction, photographed under alcohol. (**8**) Lateral view of B ray whitened with ammonium chloride. (**9**) Closeup of C ray and CD interray plating, photographed under alcohol. (**10**) Closeup of E-ray fixed brachials and intersecundibrachials showing fine rugose ornamentation on calyx plates. (**11**) Basal view of crown showing configuration of infrabasals with the CD interray oriented upward, photographed under alcohol. Scale bars = 10 mm unless otherwise noted.

https://doi.org/10.1017/jpa.2025.10110 Published online by Cambridge University Press

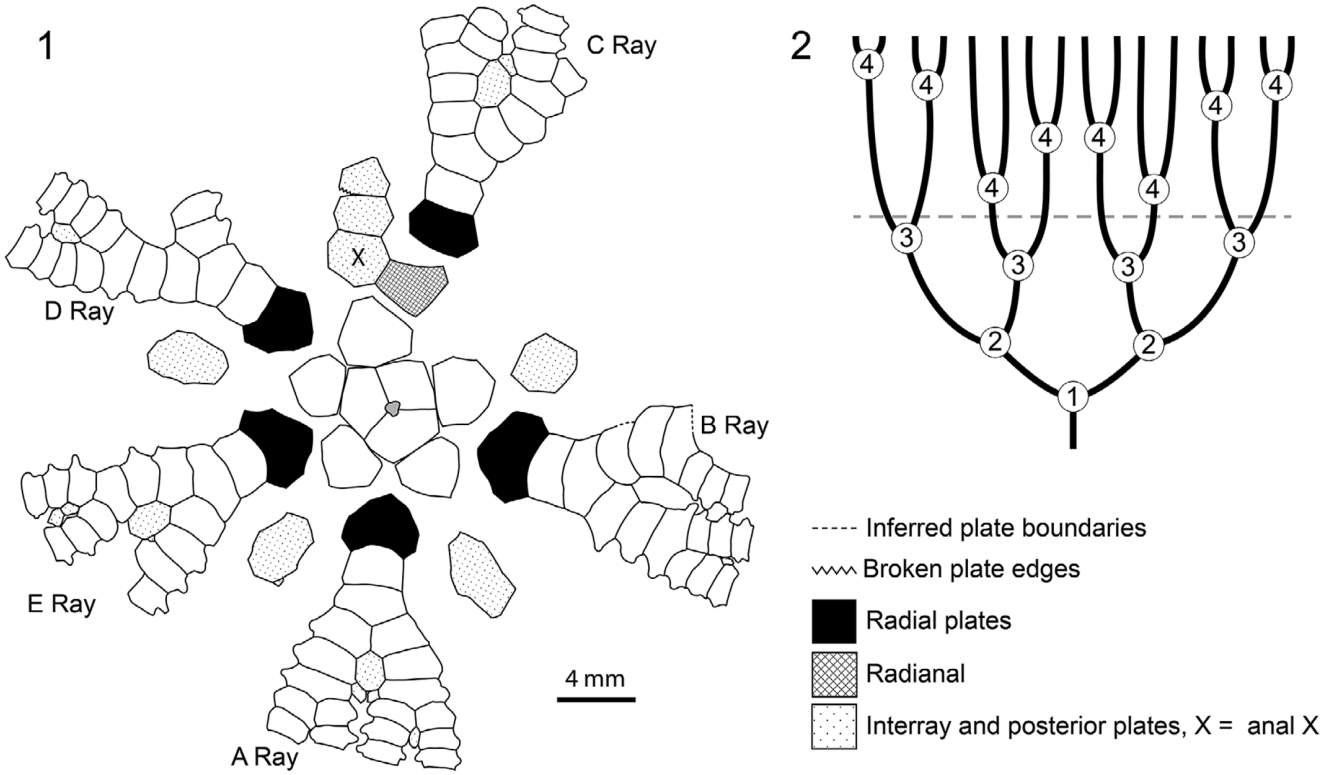

Figure 3. (**1**) Camera lucida drawing of *Anticosticrinus natiscotecensis* n. gen. n. sp., AMNH-FI-139850. (**2**) Diagrammatic representation of variability in arm branching pattern in *A. natiscotecensis*, with numbers reflecting equivalent branching points at different heights between subrays; dashed horizontal line indicates approximate transition from fixed to free brachials.

ichnogenus *Oichnus* Bromley, 1981. It is uniformly circular in outline, slightly sunken, and appears to penetrate into the plate sharply at a 90° angle. It is unknown whether the hole extends completely through the radial plate to the interior of the calyx. The black material within the boring is softer than that of the surrounding calcite plate, suggesting that it is composed of a different material that infilled the opening. The remarkably uniform, circular shape of the marking on the B radial and its apparent extension into the calyx plate support the interpretation of this feature as the trace fossil *Oichnus*, which would have formed as a result of a predatory or parasitic interaction (Baumiller, 1990; Donovan, 2017). Because of the sharp angle of penetration without any associated swelling, the morphology of the feature is more consistent with that of a boring produced by an organism such as a platycerid gastropod rather than a parasitic pit or embedment structure (Thomka and Brett, 2021). While a definite origin for this boring cannot be assigned, platycerid–crinoid associations have been recognized from the Middle Ordovician through the Permian (Baumiller and Gahn, 2002), which is consistent with the age of *A. natiscotecensis*.

The second marking is located on the second E-ray tertibrachial on the admedial side of the quarter ray (Fig. 2.6). In contrast with the marking on the B radial, the marking on the E ray is slightly irregular in outline and is slightly raised from the surface of the plate. As such, it appears to be primarily a surficial feature that does not penetrate into the plate. Although the origin of the structure is unknown, the smooth surface texture rules out the possibility of it being formed by a number of encrusting organisms, such as bryozoans.

Results

Phylogenetic results. Parsimony analysis recovered two most-parsimonious trees (MPTs) with a tree length of 34 character changes, which produced a well-resolved consensus tree with two minor polytomies (Fig. 4). In both MPTs, *Anticosticrinus* is recovered as sister to *Anisocrinus*, and *Kyphosocrinus* is consistently recovered as sister to the *Anisocrinus–Anticosticrinus* group; these relationships have relatively high jackknife and bootstrap support. *Proanisocrinus* is also recovered as being closely related to this clade, although exact placement is variable between recovered MPTs. Results of the Bayesian analysis are largely congruent with those of the parsimony analysis, including support for the sister relationship between *Anticosticrinus* and *Anisocrinus.* Combined, these results reflect phylogenetic support for family Anisocrinidae and assignment of *Anticosticrinus* to this family, which is consistent with evidence from skeletal morphology.

Divergence dating results. The 50% majority-rule tree resulting from the Bayesian divergence dating analysis is presented in Figure 5. The ages of deep nodes in the tree are slighter older than those found by a previous study (Wright and Toom, 2017), likely reflecting different interpretations of the phylogenetic position of *Cupulocrinus* within the Flexibilia (Wright et al., 2019). However, the highest posterior densities of shallow nodes and tip age distributions are broadly similar to previous results. Divergence dating analyses placed uniform prior distributions on stratigraphic ages for each species, with the boundaries for *Anticosticrinus* constrained by the geologic and geographic context of where the specimen was recovered in float. Notably, the uniform prior on

https://doi.org/10.1017/jpa.2025.10110 Published online by Cambridge University Press

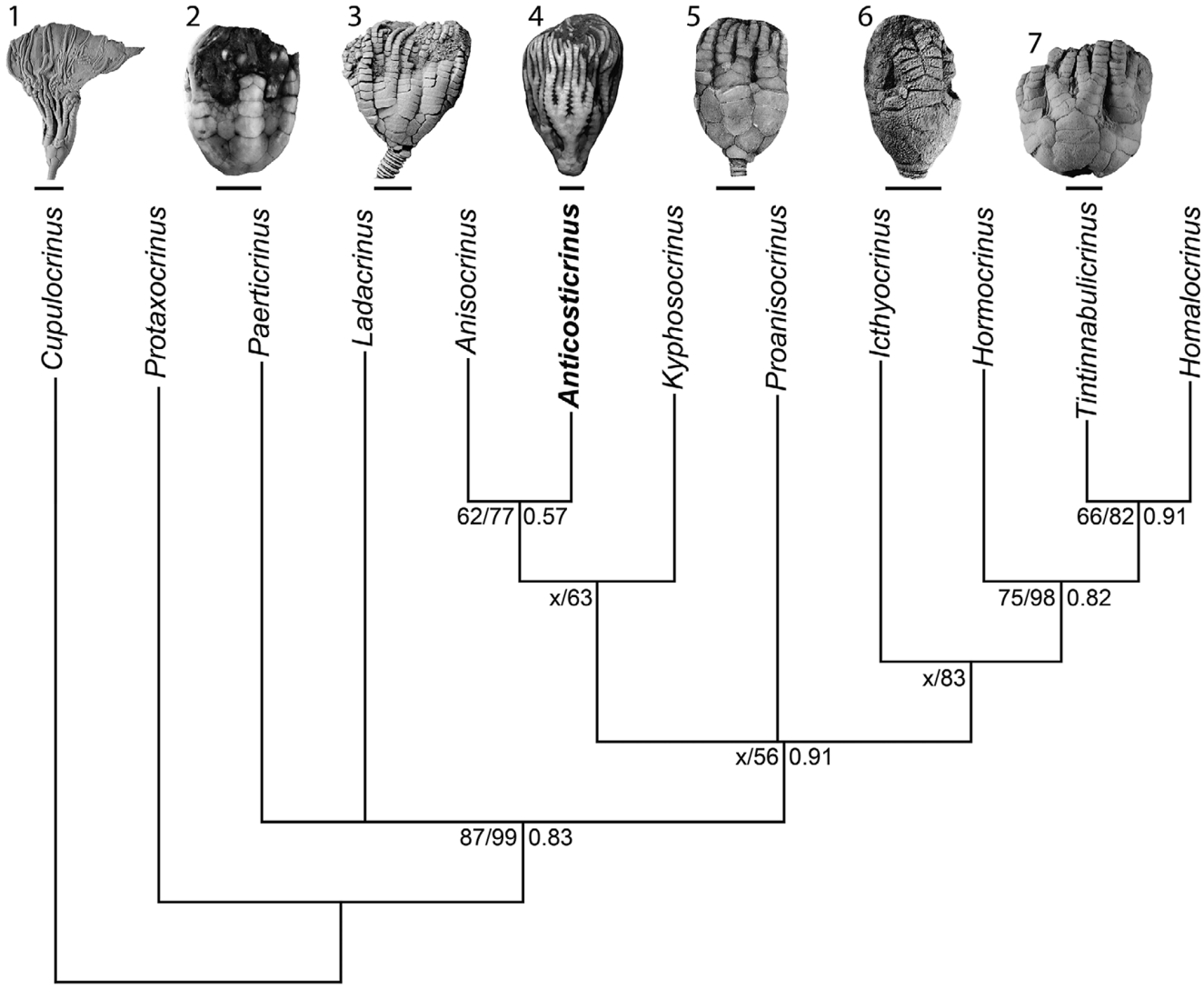

Figure 4. Strict consensus of two most-parsimonious trees summarizing the relationship of *Anticosticrinus* n. gen. to other Ordovician and early Silurian flexibles. Values at nodes are support metrics from parsimony and Bayesian phylogenetic analyses with bootstrap/jackknife support given to the left of nodes and posterior probabilities given to the right of nodes. Images correspond to representative specimens from sampled genera. (**1**) *Cupulocrinus humilis* (Billings, 1857), UMMP 74761. (**2**) *Paerticrinus arvosus* Wright and Toom, 2017, GIT 405-255. (**3**) *Anisocrinus prinstaensis*, GSC 126718 (image courtesy of W.I. Ausich). (**4**) *Anticosticrinus natiscotecensis* n. gen. n. sp., AMNH-FI-139850. (**5**) *Kyphosocrinus tetreaulti*, BMS E26377 (reproduced from Eckert and Brett, 2001 with permission from the Paleontological Research Institution, Ithaca, NY). (**6**) *Proanisocrinus oswegoensis* (Miller and Gurley, 1894), UC 6123 (reproduced from Brower, 2001 with permission from Journal of Paleontology). (**7**) *Tintinnabulicrinus estoniensis* Wright and Toom, 2017, GIT 563-3. Scale bars = 5 mm.

Anticosticrinus creates a strong bias toward recovering Silurian ages due to the unequal duration of stratigraphic intervals in which the specimen could have possibly been found. Nevertheless, the marginal posterior distribution of the stratigraphic age of *Anticosticrinus* differs significantly from a uniform distribution and instead places a greater weight of probability density on Ordovician-aged occurrences (Kolmogorov-Smirnoff test, $D = 0.087$, $P < 0.001$) (Fig. 6). The maximum a posteriori probability (MAP) estimate for the age of *Anticosticrinus*, which represents a Bayesian point estimate analogous to maximum likelihood optimization, is 444.8 Ma, placing the occurrence in the Hirnantian. Although substantial uncertainty remains surrounding its precise age (Fig. 6), and therefore does not probabilistically rule out an early Silurian age, our divergence dating analysis provides positive support for a late Hirnantian occurrence for *Anticosticrinus natiscotecensis*.

Discussion

It is well established that crinoids experienced a major faunal turnover event between the Ordovician and Silurian (Ausich et al., 1994; Ausich and Deline, 2012) in addition to significant extinction across the LOME (Ausich and Peters, 2005). However, sparse sampling across the Ordovician–Silurian boundary has made it challenging to identify the timing of this faunal transition and the mechanisms driving it, including whether the LOME served as the primary trigger for the transition or whether it served to intensify ecologically driven turnover that began before the mass extinction (Ausich and Deline, 2012; Cole and Wright, 2022). Likewise, the Katian–Hirnantian boundary has been identified as the primary interval of extinction for crinoids during the LOME rather than the Hirnantian–Silurian boundary (Ausich and Peters, 2005), but it is possible that this reflects known biases such as incomplete sampling and/or the effect of

https://doi.org/10.1017/jpa.2025.10110 Published online by Cambridge University Press

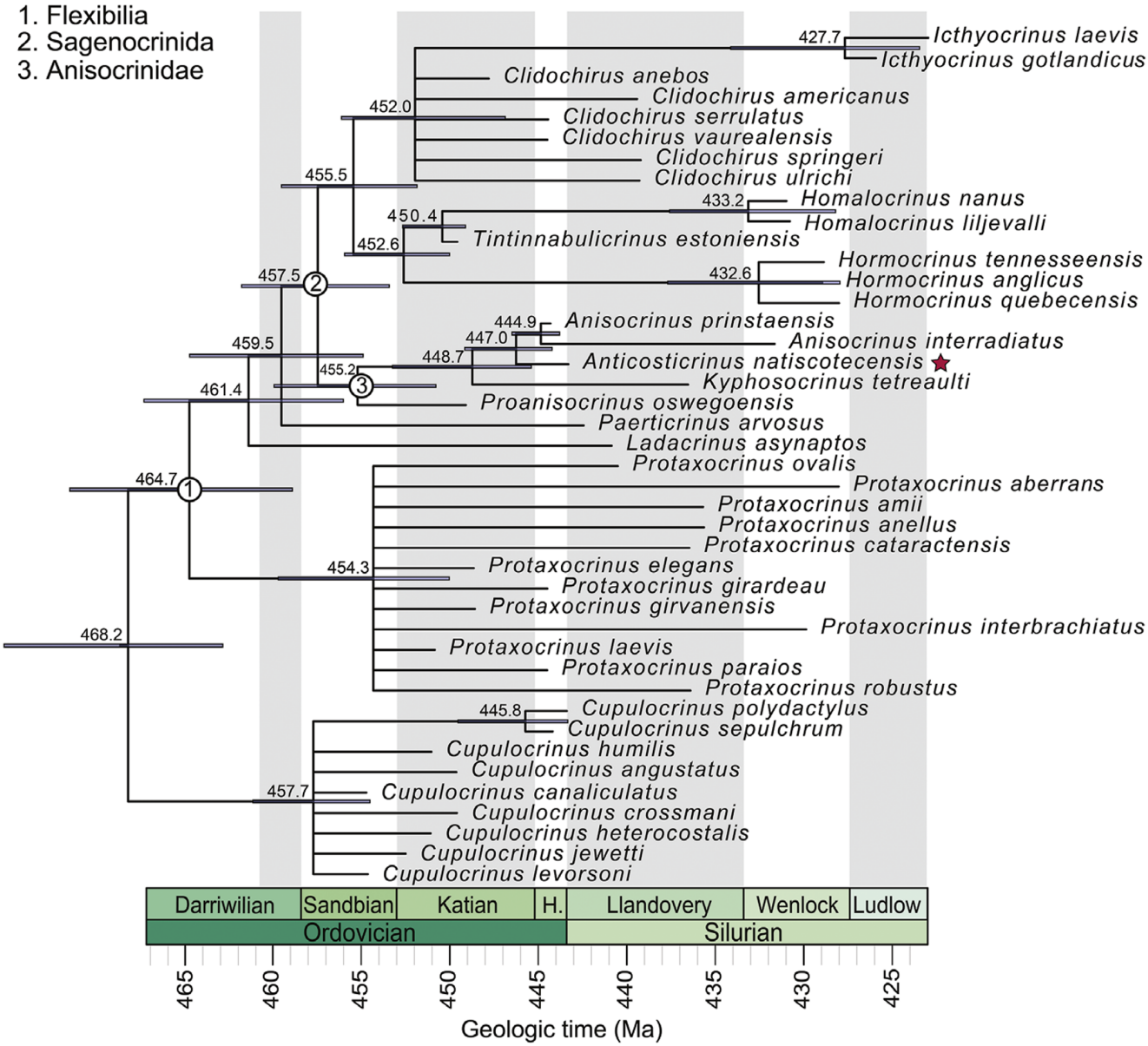

Figure 5. Tip-dated 50% majority rule phylogeny of Ordovician–Silurian flexible crinoids based on the Bayesian analysis incorporating the FBD process. Bars indicate 95% highest posterior density intervals for node ages. Numbers indicate median node ages. The star indicates the phylogenetic position of *Anticosticrinus natiscotecensis* n. gen. n. sp. H. = Hirnantian.

stratigraphic architecture on patterns of last occurrences (Holland and Patzkowsky, 2015; Zimmt et al., 2021). Thus, improved sampling during the Hirnantian and earliest Silurian is essential for constraining the timing and magnitude of crinoid extinction and faunal turnover surrounding the Ordovician–Silurian boundary.

As one of the major groups that rose to dominance during the Silurian as part of the middle Paleozoic CEF, flexible crinoids are of particular significance for understanding this interval of faunal turnover and extinction. Despite some uncertainty in its precise age, the discovery of the new flexible anisocrinid, *Anticosticrinus natiscotecensis* n. gen. n. sp. from the Ordovician–Silurian boundary interval provides additional data for evaluating this shift between the Early and Middle Crinoid Evolutionary Faunas and the timing of crinoid extinction surrounding the LOME. Remarkably, the discovery of a second Hirnantian–Rhuddanian anisocrinid in addition to *Anisocrinus prinstaensis* from the Hirnantian of Anticosti Island (Ausich and Copper, 2010) suggests that the lineage was actively diversifying in the immediate aftermath of at least the first pulse of the LOME, following the initial origination of the family in the early part of the Late Ordovician. Notably, results of the Bayesian divergence dating analysis (Fig. 5) and fossil occurrence data also suggest that the Anisocrinidae was one of the only families of flexible crinoids that diversified during the Hirnantian. Combined, these results suggest that the rise of flexibles to dominance in the middle Paleozoic CEF, at least within some clades, was under way by at least the earliest Llandovery, if not earlier. Further, recognizing the presence of two anisocrinid within the Anticosti Basin also

https://doi.org/10.1017/jpa.2025.10110 Published online by Cambridge University Press

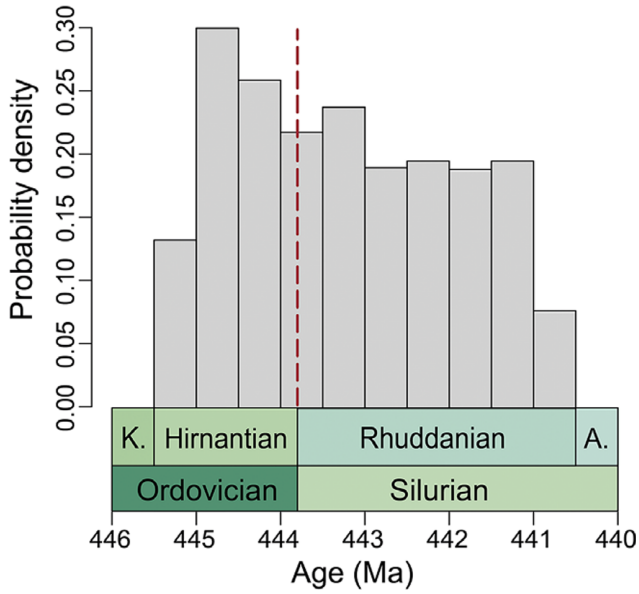

Figure 6. Probability density of age estimate for *Anticosticrinus natiscotecensis* n. gen. n. sp. recovered by the phylogenetic divergence dating analysis using the FBD process. Red vertical dashed line indicates the Ordovician–Silurian boundary. K. = Katian; A. = Aeronian.

supports the hypothesis that these groups first diversified within the paleocontinent of Laurentia before migrating to other paleocontinents such as Baltica (e.g., Ausich et al., 2024).

Data availability statement. Supplemental data are available from the Dryad Digital Repository: http://doi.org/10.5061/dryad.dz08kps8b.

Acknowledgments. We thank J. Spicer for assistance in the field, A. Desrochers for support with field logistics and access, and A. Rashkova for fossil preparation. We thank W. Ausich, F. Gahn, P. Gorzelak, and S. Zamora for providing comments that improved this manuscript. This research was supported in part by NSF EAR #2346400 to S.R.C. and D.F.W. and NSF EAR #2346401 to M.J.H. The specimen included in this study was collected and accessioned with permission of the Director General of the Municipality of Anticosti Island under Authorization Certificate F 2019-2.

Competing interests. The authors declare none.

References

Alroy, J., Aberhan, M., Bottjer, D.J., Foote, M., Fürsich, F.T., et al., 2008, Phanerozoic trends in the global diversity of marine invertebrates: *Science*, **v. 321**, p. 97–100.

Angelin, N.P., 1878, Iconographia Crinoideorum in stratis Sueciae Siluricis Fossilium: Holmiae, *Samson and Wallin*, **62** p.

Ausich, W.I., and Copper, P., 2010, The Crinoidea of Anticosti Island, Québec (Late Ordovician to early Silurian): Canadian Society of Petroleum Geologists, *Palaeontographica Canadiana* **29**, 157 p.

Ausich, W.I., and Deline, B., 2012, Macroevolutionary transition in crinoids following the Late Ordovician extinction event (Ordovician to early Silurian): *Palaeogeography, Palaeoclimatology, Palaeoecology*, **v. 361–362**, p. 38–48.

Ausich, W.I., and Peters, S.E., 2005, A revised macroevolutionary history for Ordovician–early Silurian crinoids: *Paleobiology*, **v. 31**, p. 538–551.

Ausich, W.I., Kammer, T.W., and Baumiller, T.K., 1994, Demise of the middle Paleozoic crinoid fauna: a single extinction event or rapid faunal turnover?: *Paleobiology*, **v. 20**, p. 345–361.

Ausich, W.I., Kammer, T.W., Rhenberg, E.C., and Wright, D.F., 2015, Early phylogeny of crinoids within the pelmatozoan clade: *Palaeontology*, **v. 58**, p. 937–952.

Ausich, W.I., Wright, D.F., Cole, S.R., and Sevastopulo, G.D., 2020, Homology of posterior interray plates in crinoids: a review and new perspectives from phylogenetics, the fossil record and development: *Palaeontology*, **v. 63**, p. 525–545.

Ausich, W.I., Wilson, M.A., and Toom, U., 2024, Early Silurian crinoid diversification on Baltica: *Euspirocrinus varbolaensis* sp. nov.: *Estonian Journal of Earth Sciences*, **v. 73**, p. 37.

Barido-Sottani, J., Van Tiel, N.M.A., Hopkins, M.J., Wright, D.F., Stadler, T., and Warnock, R.C.M., 2020, Ignoring fossil age uncertainty leads to inaccurate topology and divergence time estimates in time calibrated tree inference: *Frontiers in Ecology and Evolution*, **v. 8**, p. 1–13.

Barido-Sottani, J., Pohle, A., De Baets, K., Murdock, D., and Warnock, R.C., 2023. Putting the F into FBD analysis: tree constraints or morphological data?: *Palaeontology*, **v. 66**, n. e12679.

Baumiller, T.K., 1990, Non-predatory drilling of Mississippian crinoids by platyceratid gastropods: *Palaeontology*, **v. 33**, p. 743–748.

Baumiller, T.K., 1992, Major extinction events in the record of Paleozoic crinoids: new metrics for measuring extinction intensities: *Geological Society of America Abstracts with Programs*, **v. 24**, p. A95.

Baumiller, T.K., and Gahn, F.J., 2002, Fossil record of parasitism on marine invertebrates with special emphasis on the platyceratid–crinoid interaction: *The Paleontological Society Papers*, **v. 8**, p. 195–210.

Billings, E., 1857, New species of fossils from Silurian rocks of Canada: Canada Geological Survey, Report of Progress 1853–1856, Report for the year 1856, p. 247–345.

Borths, M.R., and Ausich, W.I., 2011, Ordovician–Silurian Lilliput crinoids during the end-Ordovician biotic crisis: *Swiss Journal of Palaeontology*, **v. 130**, p. 7–18.

Bromley, R.G., 1981, Concepts in ichnology illustrated by small round holes in shells: *Acta Geologica Hispanica*, **v. 16**, p. 55–64.

Brower, J.C., 2001, Flexible crinoids from the Upper Ordovician Maquoketa Formation of the northern midcontinent and the evolution of early flexible crinoids: *Journal of Paleontology*, **v. 75**, p. 370–382.

Chatterton, B.D.E., and Ludvigsen, R., 2004, Early Silurian trilobites of Anticosti Island, Québec, Canada: *Canadian Society of Petroleum Geologists, Palaeontographica Canadiana* **22**, 264 p.

Cohen, K.M., Harper, D.A.T., and Gibbard, P.L., 2023, ICS International Chronostratigraphic Chart 2023/09: International Commission on Stratigraphy, IUGS, www.stratigraphy.org.

Cole, S.R., 2019, Phylogeny and evolutionary history of diplobathrid crinoids (Echinodermata): *Palaeontology*, **v. 62**, p. 357–373.

Cole, S.R., and Wright, D.F., 2022, *Niche Evolution and Phylogenetic Community Paleoecology of Late Ordovician Crinoids*: Cambridge, UK, Cambridge University Press, 45 p.

Cole, S.R., Wright, D.F., and Ausich, W.I., 2019, Phylogenetic community paleoecology of one of the earliest complex crinoid faunas (Brechin Lagerstätte, Ordovician): *Palaeogeography, Palaeoclimatology, Palaeoecology*, **v. 521**, p. 82–98.

Cole, S.R., Wright, D.F., Ausich, W.I., and Koniecki, J.M., 2020. Paleocommunity composition, relative abundance, and new camerate crinoids from the Brechin Lagerstätte (Upper Ordovician): *Journal of Paleontology*, **v. 94**, p. 1103–1123.

Deline, B., and Ausich, W.I., 2011, Testing the plateau: a reexamination of disparity and morphologic constraints in early Paleozoic crinoids: *Paleobiology*, **v. 37**, p. 214–236.

Desrochers, A., Farley, C., Achab, A., Asselin, E., and Riva, J.F., 2010, A far-field record of the end Ordovician glaciation: the Ellis Bay Formation, Anticosti Island, Eastern Canada: *Palaeogeography, Palaeoclimatology, Palaeoecology*, **v. 296**, p. 248–263.

Donovan, S.K., 2017, A plea not to ignore ichnotaxonomy: recognizing and recording Oichnus Bromley: *Swiss Journal of Palaeontology*, **v. 136**, p. 369–372.

Donovan, S.K., Doyle, E.N., and Harper, D.A.T., 1992, A flexible crinoid from the Llandovery (Silurian) of western Ireland: *Journal of Paleontology*, **v. 66**, p. 262–266.

Eckert, J.D., and Brett, C., 2001, Early Silurian (Llandovery) crinoids from the lower Clinton Group, western New York State: *Bulletins of American Paleontology*, **v. 360**, p. 1–88.

Foote, M., 1995, Morphological diversification of Paleozoic crinoids: *Paleobiology*, **v. 21**, p. 273–299.

Foote, M., 1999, Morphological diversity in the evolutionary radiation of Paleozoic and post-Paleozoic crinoids: *Paleobiology*, **v. 25**, p. 1–115.

Frest, T.J., and Strimple, H.L., 1978, The flexible crinoid genus Anisocrinus (Ordovician–Silurian) in North America: *Journal of Paleontology*, **v. 52**, p. 683–696.

Gavryushkina, A., **Welch, D.**, **Stadler, T., and Drummond, A.J.**, 2014, Bayesian inference of sampled ancestor trees for epidemiology and fossil calibration: *PloS Computational Biology*, **v. 10**, n. e1003919.

Harper, D.A.T., **Hammarlund, E.U., and Rasmussen, C.M.Ø.**, 2014, End Ordovician extinctions: a coincidence of causes: *Gondwana Research*, **v. 25**, p. 1294–1307.

Harries, P.J., and Knorr, P.O., 2009, What does the 'Lilliput Effect' mean?: Palaeogeography, Palaeoclimatology, *Palaeoecology*, **v. 284**, p. 4–10.

Heath, T.A., **Huelsenbeck, J.P., and Stadler, T.**, 2014, The fossilized birth–death process for coherent calibration of divergence-time estimates: *Proceedings of the National Academy of Sciences*, **v. 111**, p. E2957–E2966.

Holland, S.M., and Patzkowsky, M.E., 2015, The stratigraphy of mass extinction: *Palaeontology*, **v. 58**, p. 903–924.

Jaekel, O., 1918, Phylogenie und System der Pelmatozoen: *Paläontologische Zeitschrift*, **v. 3**, p. 1–128.

Jin, J., and Zhan, R.B., 2008, *Late Ordovician orthide and billingsellide brachiopods from Anticosti Island, eastern Canada: diversity change through mass extinction*: Ottawa, Canada, NRC Research Press, 159 p.

Lepage, T., **Bryant, D.**, **Philippe, H., and Lartillot, N.**, 2007, A general comparison of relaxed molecular clock models: *Molecular Biology and Evolution*, **v. 24**, p. 2669–2680.

Lewis, P.O., 2001, A likelihood approach to estimating phylogeny from discrete morphological character data: *Systematic Biology*, **v. 50**, p. 913–925.

Long, D.G.F., 2007, Tempestite frequency curves: a key to Late Ordovician and early Silurian subsidence, sea-level change, and orbital forcing in the Anticosti foreland basin, Québec, Canada: *Canadian Journal of Earth Sciences*, **v. 44**, p. 413–431.

Mauviel, A., **Sinnesael, M., and Desrochers, A.**, 2020, The stratigraphic and geochemical imprints of Late Ordovician glaciation on far-field neritic carbonates, Anticosti Island, eastern Canada: *Palaeogeography, Palaeoclimatology, Palaeoecology*, **v. 543**, n. 109579.

Miller, J.S., 1821, *A Natural History of the Crinoidea, or Lily-Shaped Animals; with Observations on the Genera,* Asteria, Euryale, Comatula *and* Marsupites: Bristol, England, Bryan and Co., 150 p.

Miller, S. A., and Gurley, W.F.E., 1894, Upper Devonian and Niagara crinoids: *Illinois State Museum Bulletin* **4**, p. 1–37.

Moore, R.C., and Laudon, L.R., 1943, Evolution and classification of Paleozoic crinoids: *Geological Society of America Special Papers* **46**, 154 p.

Novack-Gottshall, P.M., **Sultan, A.**, **Smith, N.S.**, **Purcell, J.**, **Hanson, K.E.**, et al., 2022, Morphological volatility precedes ecological innovation in early echinoderms: *Nature Ecology and Evolution*, **v. 6**, p. 263–272.

Novack-Gottshall, P.M., **Purcell, J.**, **Sultan, A.**, **Ranjha, I.**, **Deline, B., and Sumrall, C.D.**, 2024, Ecological novelty at the start of the Cambrian and Ordovician radiations of echinoderms: *Palaeontology*, **v. 67**, n. e12688.

Peters, S.E., and Ausich, W.I., 2008, A sampling-adjusted macroevolutionary history for Ordovician–early Silurian crinoids: *Paleobiology*, **v. 34**, p. 104–116.

Rambaut, A., **Drummond, A.J.**, **Xie, D.**, **Baele, G., and Suchard, M.A.**, 2018, Posterior summarization in Bayesian phylogenetics using Tracer 1.7: *Systematic Biology*, **v. 67**, p. 901–904.

Rannala, B., **Zhu, T., and Yang, Z.**, 2012, Tail paradox, partial identifiability, and influential priors in Bayesian branch length inference: *Molecular Biology and Evolution*, **v. 29**, p. 325–335.

Roemer, C.F., 1854–1855, Erste Periode, Kohlen-Gebirge, *in* Bronn, H.G., ed., *Lethaea Geognostica* (third edition), Volume **2**: Stuttgart, E. Schweizerbart, 788 p.

Ronquist, F., **Klopfstein, S.**, **Vilhelmsen, L.**, **Schulmeister, S.**, **Murray, D.L., and Rasnitsyn, A.P.**, 2012, A total-evidence approach to dating with fossils, applied to the early radiation of the Hymenoptera: *Systematic Biology*, **v. 61**, p. 973–999.

Salamon, M.A., **Brachaniec, T.**, **Paszcza, K.**, **Kołbuk, D., and Gorzelak, P.**, 2023, The role of mass extinction events in shaping the body-size dynamics of fossil crinoids: *Palaeogeography, Palaeoclimatology, Palaeoecology*, **v. 622**, n. 111593.

Sepkoski, J.J., 1996, Patterns of Phanerozoic extinction: a perspective from global data bases, *in* Walliser, O.H., ed., *Global Events and Event Stratigraphy in the Phanerozoic*: Berlin and Heidelberg, Springer, p. 35–51.

Springer, F., 1913, Crinoidea, *in* von Zittel, K.A., ed., *Text-book of Paleontology* (second edition): London, Macmillan, p. 971.

Springer, F., 1920, *The Crinoidea Flexibilia (with an Atlas of A., B., C., and 76 Plates)*: Washington, D.C., Smithsonian Institution, 504 p.

Stadler, T., 2010, Sampling-through-time in birth–death trees: *Journal of Theoretical Biology*, **v. 267**, p. 396–404.

Swofford, D.L., 2003, PAUP*: phylogenetic analysis using parsimony (*and other methods), Version 4: *Sunderland, Massachusetts, Sinauer Associates*.

Thomka, J.R., and Brett, C.E., 2021, Parasitism of Paleozoic crinoids and related stalked echinoderms: paleopathology, ichnology, coevolution, and evolutionary paleoecology, *in* De Baets, K., and Huntley, J.W., eds., *The Evolution and Fossil Record of Parasitism*: Cham, Switzerland, Springer, p. 289–316.

Ubaghs, G., 1978, General morphology, *in* Moore, R.C., and Teichert, C., eds., *Treatise on Invertebrate Paleontology*, Part T, Echinodermata 2: Lawrence, Kansas, Geological Society of America and University of Kansas Press, p. T58–T216.

Von Zittel, K.A., 1895, Grundzüge Der Paläontologie (Paläzoologie): München und Berlin, Druck und Verlag von R. Oldenbourg, 971 p.

Wachsmuth, C., and Springer, F., 1885, Revision of the Palaeocrinoidea Pt. III, Sec. 1. Discussion of the Classification and Relations of the Brachiate Crinoids, and Conclusion of the Generic Descriptions: Proceedings of the Academy of Natural Sciences of Philadelphia, p. 225–364.

Wright, A., **Wagner, P.J., and Wright, D.F.**, 2021, *Testing Character Evolution Models in Phylogenetic Paleobiology: A Case Study with Cambrian Echinoderms*: Cambridge, UK, Cambridge University Press, 42 p.

Wright, D.F., 2015, Fossils, homology, and "Phylogenetic Paleo-ontogeny": a reassessment of primary posterior plate homologies among fossil and living crinoids with insights from developmental biology: *Paleobiology*, **v. 41**, p. 570–591.

Wright, D.F., 2017, Bayesian estimation of fossil phylogenies and the evolution of early to middle Paleozoic crinoids (Echinodermata): *Journal of Paleontology*, **v. 91**, p. 799–814.

Wright, D.F., and Toom, U., 2017, New crinoids from the Baltic region (Estonia): fossil tip-dating phylogenetics constrains the origin and Ordovician–Silurian diversification of the Flexibilia (Echinodermata): *Palaeontology*, **v. 60**, p. 893–910.

Wright, D.F., **Ausich, W.I.**, **Cole, S.R.**, **Peter, M.E., and Rhenberg, E.C.**, 2017, Phylogenetic taxonomy and classification of the Crinoidea (Echinodermata): *Journal of Paleontology*, **v. 91**, p. 829–846.

Wright, D.F., **Cole, S.R., and Ausich, W.I.**, 2019. Biodiversity, systematics, and new taxa of cladid crinoids from the Ordovician Brechin Lagerstätte: *Journal of Paleontology*, **v. 94**, p. 334–357.

Zhang, C., **Rannala, B., and Yang, Z.**, 2012, Robustness of compound Dirichlet priors for Bayesian inference of branch lengths: *Systematic Biology*, **v. 61**, p. 779–784.

Zimmt, J.B., **Holland, S.M.**, **Finnegan, S., and Marshall, C.R.**, 2021, Recognizing pulses of extinction from clusters of last occurrences: *Palaeontology*, **v. 64**, p. 1–20.

https://doi.org/10.1017/jpa.2025.10110 Published online by Cambridge University Press